

---

# Is Attention Required for Transformer Inference? Explore Function-preserving Attention Replacement

---

**Yuxin Ren**  
University of Arizona  
Tucson, AZ 85721  
yuxinr@arizona.edu

**Maxwell D Collins**  
TetraMem, Inc.  
1251 McKay Dr.  
San Jose, CA 95133, USA  
maxwell.collins@tetramem.com

**Miao Hu**  
TetraMem, Inc.  
1251 McKay Dr.  
San Jose, CA 95133, USA  
miao.hu@tetramem.com

**Huanrui Yang\***  
University of Arizona  
Tucson, AZ 85721  
huanruiyang@arizona.edu

## Abstract

While transformers excel across vision and language pretraining tasks, their reliance on attention mechanisms poses challenges for inference efficiency, especially on edge and embedded accelerators with limited parallelism and memory bandwidth. Hinted by the observed redundancy of attention at inference time, we hypothesize that though the model learns complicated token dependency through pretraining, the inference-time sequence-to-sequence mapping in each attention layer is actually “simple” enough to be represented with a much cheaper function. In this work, we explore FAR, a Function-preserving Attention Replacement framework that replaces all attention blocks in pretrained transformers with learnable sequence-to-sequence modules, exemplified by an LSTM. FAR optimizes a multi-head LSTM architecture with a block-wise distillation objective and a global structural pruning framework to achieve a family of efficient LSTM-based models from pretrained transformers. We validate FAR on the DeiT vision transformer family and demonstrate that it matches the accuracy of the original models on ImageNet and multiple downstream tasks with reduced parameters and latency. Further analysis shows that FAR preserves the semantic token relationships and the token-to-token correlation learned in the transformer’s attention module.

## 1 Introduction

Transformer models have become the foundation of state-of-the-art architectures across natural language processing, vision, and multimodal learning [1–4]. Their success is largely attributed to the self-attention mechanism, which enables modeling long-range dependencies and rich contextual interactions through large-scale pretraining [5]. While attention excels during training on highly parallel hardware, such as GPUs and TPUs, it introduces significant challenges at inference time: its quadratic cost in sequence length and reliance on global token interactions lead to poor runtime efficiency on devices with limited parallelism [6, 7]. Even with further approximations like linear attention [8] or Mamba [9] modules, the on-the-fly activation-to-activation multiplications in the attention mechanism is unavoidably leading to poor data reuse and requiring significant memory access, hindering its efficient deployment on accelerators with emerging memory like ReRAM [10, 11] that has limited bandwidth in memory reading or writing.

---

\*Corresponding author.

Though full attention is required in large-scale pretraining, recent observations of pretrained transformers have revealed redundancy across attention layers at inference time, demonstrated by the sparse attention pattern even without explicit regularization [12, 13]. This phenomena hints that not all attention layers are learning a complicated sequence-to-sequence mapping through the pretraining process. Rather, the pretraining decomposes the complicated end-to-end mapping into a series of much simpler sequence-to-sequence transformations in each attention layer.

**Hypothesis.** We hypothesize that the large-scale pretraining implicitly decomposes complex dependencies into simpler layer-wise token interactions. Consequently, while attention is indispensable during training, its behavior during inference can be approximated by simpler sequential modules, provided that they are properly supervised to capture the learned token interactions. Based on this hypothesis, we explore whether it is possible to replace attention blocks in pretrained transformers with efficient alternatives, without sacrificing model performance.

To test this hypothesis, we propose **FAR**, a function-preserving attention replacement framework that substitutes each attention block in a pretrained transformer with a learnable sequence-to-sequence module. While FAR can in principle accommodate any substitute sequence-to-sequence model architecture, we use bidirectional LSTM [14] as the substitute block in this work, showcasing that an architecture typically believed to be not suitable for large-scale pretraining can learn well under distillation. The substitute blocks are trained to mimic the input-output behavior of the original attention via blockwise distillation. To ensure stable convergence, we replace all attention blocks simultaneously and supervise each replacement with a similarity-based objective. The rest of the model remains frozen, preserving compatibility with the pre-trained weights and allowing selective substitution without retraining from scratch. To better capture the difference in difficulties of the distillation objective across the blocks, we incorporate sparsity-inducing regularizations [15] to dynamically prune the substitute blocks into suitable capacity to learn the sequence-to-sequence mapping of the corresponding attention block.

We validate FAR on the DeiT [16] vision transformer family and show that it preserves the accuracy scaling behavior of attention-based models across model sizes. Notably, on smaller variants like DeiT-Tiny, FAR even slightly surpasses the original model, while maintaining comparable performance on DeiT-Small and DeiT-Base. FAR models distilled from pretrained ImageNet model also show good generalizability when finetuned to downstream classification tasks including CIFAR, Flowers, Cars, and iNaturalist, indicating that the learned sequence-to-sequence mappings remain effective across domains. Besides similar performance, FAR models match or reduce the model size compared with the original DeiT model and consistently lower FLOPs, leading to a lowered inference latency on CPUs with gains growing as sequence length increases, well-suited for deployment on resource-constrained hardware.

In summary, FAR provides a general architecture replacement framework to achieve efficient, attention-free inference of pretrained transformers, bridging structural replacement, localized distillation, and model compression under a unified method.

## 2 Related Work

**Efficient Alternatives to Self-Attention.** The quadratic complexity of self-attention has spurred the development of both attention-free and attention-efficient architectures. Attention-free models such as MLP-Mixer [17], RetNet [18], and Mamba [19] replace attention with token-mixing mechanisms based on MLPs, implicit recurrence, or state-space models, offering linear complexity and improved hardware efficiency. However, these architectures are typically trained from scratch with bespoke recipes and remain incompatible with pre-trained transformers, limiting their transferability and scalability. In parallel, efficient attention variants attempt to reduce the runtime and memory overhead of the original mechanism. Linformer [20] and Performer [21] approximate softmax attention via low-rank projections or kernel-based methods, while FlashAttention [22] and Reformer [23] improve performance through kernel fusion or weight sharing. Despite these improvements, most designs preserve the core all-pairs interaction and dynamic memory patterns of attention, which remain suboptimal for deployment on memory-constrained hardware. Our work diverges from both lines by eliminating attention altogether at inference time and replacing it with a sequential structure trained to replicate the functional behavior of the original network.

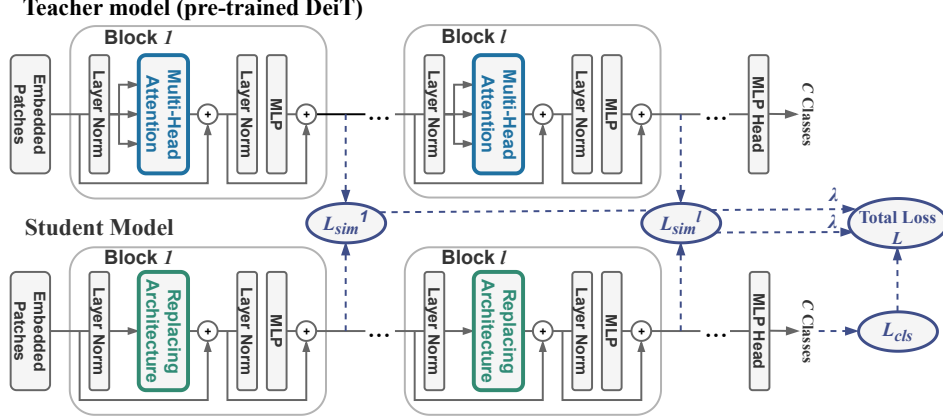


Figure 1: Illustration of the proposed attention replacement strategy. Each replaced block (green) is supervised by a similarity loss, and a classification loss is applied to the final output. During distillation, only the replaced block are trainable, with all other weights frozen.

**Distillation and Modular Replacement.** Knowledge distillation [24] is a widely adopted technique for transferring information from large models to compact ones. Beyond end-to-end supervision, several studies explore layer-wise or block-wise distillation to facilitate architectural flexibility. TinyBERT [25], MobileBERT [26] and MiniLM [27] apply intermediate-level supervision to compress transformers without retraining from scratch. LayerDrop [28] introduces random layer skipping during training, enabling dynamic pruning at inference. While these approaches aim at efficiency, they generally preserve the attention structure or require retraining the entire model. Our method departs from this by freezing the pre-trained transformer and distilling the behavior of each attention block into a lightweight recurrent substitute, enabling structural replacement without compromising compatibility or transferability.

### 3 Function-preserving Attention Replacement

#### 3.1 Replacement Strategy

Figure 1 provides an overview of our proposed attention replacement framework. We replace attention blocks in a pre-trained vision transformer with learnable sequential modules supervised via both the block-level distillation and the global task loss.

We consider a pretrained vision transformer (e.g., DeiT) composed of  $L$  layers, where each layer consists of an attention block  $A_l$  and a feedforward block  $F_l$ , connected via residual paths and layer normalization. The  $l$ -th layer processes input  $\mathbf{x}_l \in \mathbb{R}^{T \times h}$  (where  $T$  is the sequence length and  $h$  is the embedding size) as:

$$\mathbf{y}_l = \mathbf{x}_l + A_l(\text{LN}_1(\mathbf{x}_l)) ; \quad \mathbf{x}_{l+1} = \mathbf{y}_l + F_l(\text{LN}_2(\mathbf{y}_l)) \quad (1)$$

The core operation in  $A_l(\cdot)$  is the softmax attention, which computes pairwise similarity between token embeddings. This dynamic activation-to-activation multiplication incurs  $\mathcal{O}(T^2)$  complexity and impedes deployment on memory-bounded or low-parallelism hardware platforms.

Motivated by the observed redundancy and progressive smoothing of attention patterns across layers [12, 13], we hypothesize that each attention block performs a learned sequence-to-sequence transformation that can be approximated by a simpler sequential module.

Given this hypothesis, our objective is to replace each attention block  $A_l$  with a learnable substitute  $A'_l$ , such that the modified layer becomes:

$$\mathbf{y}'_l = \mathbf{x}_l + A'_l(\mathbf{x}_l) ; \quad \mathbf{x}'_{l+1} = \mathbf{y}'_l + F_l(\mathbf{y}'_l) \quad (2)$$

This design imposes the following requirements on each substitute module  $A'_l$ :

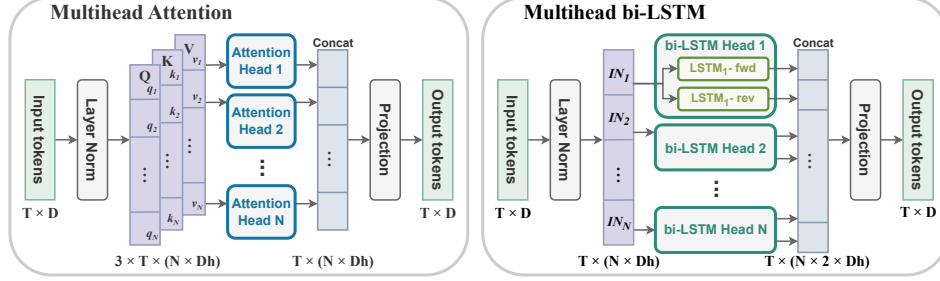


Figure 2: Multi-head bi-LSTM module used to replace attention. The input is first projected into  $N$  subspaces and split by head. Each subspace is processed by a bidirectional LSTM, and the outputs are concatenated and projected back to the original hidden size.

- **Functional equivalence:** The substitute should approximate the output of the original attention block, i.e.,  $A'_l(\mathbf{x}_l) \approx A_l(\mathbf{x}_l)$ , preserving the model’s representational behavior.
- **Plug-in compatibility:** The substitute should integrate into the pretrained model without modifying surrounding layers, enabling replacement with minimal retraining.
- **Inference efficiency:** The substitute should adopt a sequential structure more compatible with CPU execution or memory-bound accelerators, avoiding the quadratic overhead and dynamic memory access of attention.

To guide training, we supervise each  $A'_l$  via a block-level distillation loss. Let  $\mathcal{R}$  denote the set of replaced layers. For each  $i \in \mathcal{R}$ , we define the similarity loss as:

$$\mathcal{L}_{\text{sim}}^{(i)} = 1 - \cos(\mathbf{x}_{i+1}, \mathbf{x}'_{i+1}), \quad (3)$$

where  $\mathbf{x}_{i+1}$  and  $\mathbf{x}'_{i+1}$  are the outputs of the original and replaced blocks, respectively. Although we replace only the attention block, we supervise at the level of the full block output to ensure stability and downstream consistency. This supervision ensures that the substitute blocks preserve the representational behavior of the original attention modules.

The overall training objective combines both structural and task-level supervisions:

$$\mathcal{L} = \lambda \cdot \sum_{i \in \mathcal{R}} \mathcal{L}_{\text{sim}}^{(i)} + \mathcal{L}_{\text{cls}}, \quad (4)$$

where  $\mathcal{L}_{\text{cls}}$  is the cross-entropy loss in the final output and  $\lambda$  controls the trade-off.

**Training protocol.** We adopt a *global replacement* strategy: all attention blocks are substituted at once, avoiding representation mismatch that arises when partially replacing layers in sequence. Training proceeds in two stages:

- **Distillation phase:** The substitute modules are trained using the combined loss while the rest of the model is frozen.
- **Finetuning phase:** All parameters are unfrozen and jointly optimized using task supervision to recover any residual accuracy drop.

### 3.2 Multi-head LSTM Architecture

While our framework is compatible with various sequential substitutes (e.g., convolutional or state-space models), we instantiate the substitute module  $A'_l$  using a **multi-head bidirectional LSTM** (BiLSTM [14]) architecture in this work. This choice introduces recurrence into the model while preserving compatibility with the structural layout of multi-head attention, making it suitable for deployment in environments with limited parallelism or memory-centric constraints.

Our choice is motivated by two observations: (1) Bidirectional LSTMs can model forward and backward token dependencies, making them a strong candidate for capturing sequence-level representations; (2) Multi-head attention employs multiple heads to scale up the embedding size and extract diverse token interaction patterns in parallel. To preserve this inductive bias and improve scalability, we adopt a multi-head structure in our LSTM-based replacement.

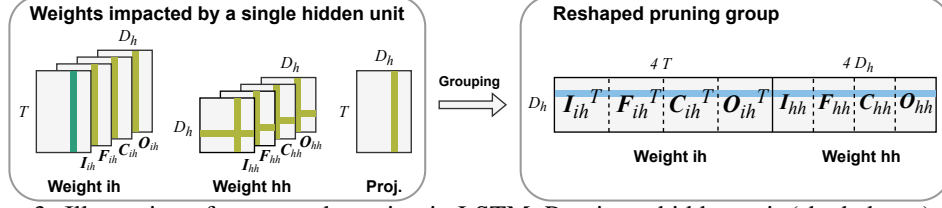


Figure 3: Illustration of structured pruning in LSTM. Pruning a hidden unit (shaded row) affects input-hidden weights, hidden-hidden weights, and downstream projections. Coordinated pruning across all gate matrices ensures consistency and avoids temporal misalignment. *While the figure shows pruning groups excluding the transpose of hidden-hidden matrices and projection layers for clarity, our framework optionally supports joint grouping over all structurally coupled parameters.*

The overall architecture is illustrated in Figure 2. Concretely, let  $\mathbf{x} \in \mathbb{R}^{T \times D}$  denote the input to the module, where  $T$  is the sequence length and  $D$  the embedding size. We first apply layer normalization and a linear projection to map the input into  $N$  subspaces of dimension  $D_h$ , such that  $D = N \cdot D_h$ . This projection replaces the QKV projection of the original attention mechanism. These projected sequences  $\{\mathbf{I}_n\}_{n=1}^N$  are then processed by  $N$  bidirectional LSTM heads in parallel, yielding  $\mathbf{H}_n = \text{BiLSTM}_n(\mathbf{I}_n) \in \mathbb{R}^{T \times 2D_h}$ , where each BiLSTM head outputs a forward and backward representation per token, which are concatenated along the embedding dimension. The outputs of all heads are then concatenated as  $\mathbf{H} = [\mathbf{H}_1; \dots; \mathbf{H}_N] \in \mathbb{R}^{T \times 2D}$ . Finally, we apply a linear projection to map  $\mathbf{H}$  back to the original input size by  $\mathbf{y} = \text{Proj}(\mathbf{H}) \in \mathbb{R}^{T \times D}$ .

This architecture mirrors the projection-split-recombine pattern of attention blocks. By structurally aligning with the original ViT backbone, it enables efficient substitution without compromising architectural compatibility. Unlike attention, it replaces all-pair token interaction with local recurrence, which scales more favorably in constrained hardware.

To ensure dimensional compatibility and retain pretraining alignment, we match the number of LSTM heads to the number of attention heads in the original DeiT model. Each head uses a hidden size equal to the per-head dimension in the corresponding attention block, ensuring structural alignment and comparable model capacity.

### 3.3 Post-distillation Compression via Structured Pruning

Both the pretrained transformer and our proposed LSTM-based substitute modules introduced in Section 3.2 takes a unified design across the blocks. However, different levels of redundancy are observed in different transformer blocks [29, 30], hinting that each of their functionality can be learned by substitute models of different capacity. To reflect such difference and ensure model compactness, we adopt structured pruning to adjust the hidden dimension of each LSTM block.

**Extension of DeepHoyer to LSTM.** To promote structured sparsity during training, we extend the DeepHoyer framework [15], which introduces a differentiable approximation to the Hoyer sparsity measure. This measure captures the sparsity of  $W$  by encouraging a few large entries while suppressing the rest. DeepHoyer generalizes Hoyer measure to Group-HS for structured sparsity using group  $\ell_2$  norms:

$$G_H(W) = \frac{\left(\sum_{g=1}^G \|w^{(g)}\|_2\right)^2}{\sum_{g=1}^G \|w^{(g)}\|_2^2}, \quad (5)$$

where each  $w^{(g)}$  denotes a group of weights (e.g., one output channel).

While originally designed for convolutional and fully connected layers, we extend this method to bidirectional LSTM modules by targeting the hidden dimension. Crucially, due to the gate structure of LSTMs, pruning a particular hidden unit requires coordinated removal across all gates and associated matrices to preserve consistency. Specifically, for each unidirectional LSTM block, we identify the set of weights influenced by a hidden unit across all four gates (input, forget, cell, and output). These include: (1) the corresponding rows in the input-to-hidden ( $W_{ih}$ ) weight matrices, (2) the corresponding rows and columns in the hidden-to-hidden ( $W_{hh}$ ) matrices, and (3) the corresponding columns for the next layer. As illustrated in Figure 3, these components are concatenated into a

composite matrix  $W^{(l)} \in \mathbb{R}^{D_h \times G}$ , where each row corresponds to one hidden unit and  $G$  denotes the total number of gate-aligned entries per unit.

We then compute the structured regularization penalty for block  $l$  across the rows of  $W^{(l)}$  to obtain structured importance scores per hidden unit:

$$\mathcal{R}_{\text{Hoyer}}^{(l)} = \frac{\left(\sum_{j=1}^{D_h} \|W^{(l)}[j, :]\|_2\right)^2}{\sum_{j=1}^{D_h} \|W^{(l)}[j, :]\|_2^2}. \quad (6)$$

This term is added to the original loss during regularized training, guiding the network towards sparse hidden representations while maintaining structural integrity across gates.

We apply structured pruning through a three-stage pipeline:

- **Regularization.** A Hoyer-based sparsity penalty is introduced to promote structured sparsity along the hidden dimension of each LSTM block. This regularization can be applied either jointly with block-level distillation or as a separate retraining stage after substitute modules are initialized.
- **Pruning.** After regularization training, we compute the row-wise group norms of  $W^{(l)}$  and prune all hidden units whose importance falls below a threshold. Since each hidden unit participates in all gate matrices, pruning is performed in a coordinated fashion across gates and associated projections.
- **Finetuning.** The pruned model is further finetuned with masked weights fixed to zero. This recovers potential accuracy degradation while preserving the compressed structure.

Structured pruning is performed independently for each LSTM block and direction, allowing layer-adaptive sparsity. Unlike global pruning with a fixed budget, this approach reflects the differing redundancy and saliency of layers. As shown in Section 4.3, we observe considerable variation in compression ratios across depth and direction, highlighting the benefit of block-wise flexibility.

## 4 Experiment results

### 4.1 Experiment Setup

We evaluate our attention replacement framework on the DeiT family of vision transformers [16], including DeiT-Tiny, DeiT-Small and DeiT-Base. For each model, the self-attention architecture of all layers are replaced with multi-head bidirectional LSTM modules. The number of heads and total width are kept the same, and the hidden dimension per head of the LSTM is set to 64 to match the original DeiT configuration. Except for the replaced part, all other components including the MLP sublayers, normalization, and embeddings retain their original pretrained weights and remain frozen during the initial training stage.

Training protocols follow the original DeiT setup as closely as possible, including the data augmentation recipe and the optimizer configuration. However, due to the nature of LSTM modules, we apply different hyperparameter settings, including learning rate and batch size, which are detailed in Appendix A.1. During the distillation, only the LSTM substitute blocks are updated using the combined loss described in Section 3.1. We set the default parameter  $\lambda = 1$  for the similarity term.

For pruning experiments, as described in Section 3.3, we apply DeepHoyer regularization to each LSTM head, performing structured pruning on the hidden dimension. The pruning is adaptive per block using threshold-based selection, with full hyperparameter details provided in Appendix A.2.

Evaluation is conducted using Top-1 classification accuracy on ImageNet [31] and several downstream datasets, including CIFAR-10/100 [32], Stanford Cars [33], and Flowers-102 [34]. For downstream transfer, we follow the DeiT finetuning protocol and objective without the teacher transformer. Dataset splits and augmentation strategies are consistent with standard practice.

We report the Top-1 accuracy, parameter count, and inference efficiency metrics including latency and FLOPs in Section 4.3. Latency is measured on an AMD EPYC 9254 CPU and 8× NVIDIA A6000 GPUs. Batch size, thread count, and measurement details are provided in Appendix A.4.

Table 1: Top-1 accuracy of DeiT and FAR models on ImageNet and downstream classification benchmarks. FAR models are trained via block-wise distillation. For downstream tasks, the pretrained FAR and DeiT models are finetuned on each task without distillation.

Model	ImageNet	CIFAR-10	CIFAR-100	Cars	Flowers
DeiT-Tiny	72.2	97.9	85.7	90.5	97.4
FAR-Tiny	74.2	97.8	85.8	88.9	97.1
FAR-Tiny <sup>†</sup>	72.5	97.1	83.3	87.0	96.5
DeiT-Small	79.8	98.5	87.1	91.7	98.1
FAR-Small	77.9	98.1	87.1	88.2	98.3
FAR-Small <sup>†</sup>	75.4	97.3	85.1	86.0	97.0
DeiT-Base	81.8	99.1	90.8	92.1	98.4
FAR-Base	79.5	98.4	88.5	89.5	98.2
FAR-Base <sup>†</sup>	77.3	97.7	86.4	87.5	97.5

<sup>†</sup> Pruned model after structured compression.

## 4.2 Main Results: Accuracy Retention

We first evaluate how well FAR preserves classification performance on ImageNet. Table 1 summarizes Top-1 accuracies across three model scales. On DeiT-Tiny, FAR matches or even exceeds the baseline: the unpruned model improves accuracy by **+2.0%**, while the pruned variant retains competitive performance with fewer parameters.

When scaling up the embedding size to DeiT-Small and Base levels, FAR models achieves consistent accuracy gains, yet fall slightly behind the teacher transformer model. This degradation is expected, as larger attention modules encode more complex token interactions that are inherently harder to replicate with sequential substitutes. Nevertheless, even under full replacement and without retraining the surrounding layers, FAR maintains competitive accuracy across scales, highlighting its potential as a structurally simplified and efficient alternative to attention.

**Generalization Across Tasks.** To assess whether FAR preserves transferable inductive biases learned from ImageNet pretraining, we evaluate its performance on a diverse set of downstream tasks. Rather than distilling from task-specific DeiT teachers, we directly finetune FAR models on each target dataset using standard supervised training protocols. This setup isolates the intrinsic transferability of the learned representations in FAR and tests whether the sequential substitute can adapt to varying token interaction patterns across domains.

As shown in Table 1, the unpruned FAR-Tiny model achieves competitive performance across all tasks, with accuracy closely tracking that of the DeiT baseline. Notably, the relative performance gap from ImageNet to downstream datasets is comparable between FAR and DeiT, indicating that the replacement of attention does not introduce additional degradation in transferability. This suggests that FAR retains the inductive structure and generalization trends of attention-based models.

**Summary.** Across both pretraining and transfer settings, FAR shows that attention blocks in transformers can be replaced with simpler sequential modules while maintaining reasonable performance. The proposed substitutes offer a drop-in alternative that preserves much of the original model’s behavior, without requiring task-specific distillation or full-model retraining.

## 4.3 Efficiency and Behavioral Analysis

We analyze the efficiency and internal behavior of FAR, complementing the accuracy evaluation with practical and interpretability-driven assessments. Our goals are to: (1) verify whether FAR improves inference efficiency over attention-based counterparts; (2) assess its representation quality and alignment with attention; and (3) understand the effect of distillation and structured pruning on training dynamics and sparsity.

**Inference Efficiency and Structured Compression.** Table 2 reports the model size, FLOPs, and measured inference latency for DeiT and FAR variants across image resolutions and hardware settings. While the unpruned FAR variants introduce moderate parameter overhead due to recurrent blocks, structured pruning (Section 3.3) effectively reduces both model size and computation.

Table 2: Model size, FLOPs, and inference latency for DeiT and FAR variants. FLOPs and latency measured on both  $224 \times 224$  and  $384 \times 384$  images; latency averaged over 100 runs on target device.

Model	Params (M)	FLOPs 224(G)	FLOPs 384(G)	Latency* CPU 224 (ms)	Latency* CPU 384 (ms)
DeiT-Tiny	5.7	1.25	4.63	26.51	103.02
FAR-Tiny	7.7	1.45	4.20	33.78	93.37
FAR-Tiny <sup>†</sup>	5.7	1.08	3.12	30.95	89.44
DeiT-Small	22.1	4.60	15.49	84.37	285.83
FAR-Small	24.9	4.82	14.12	91.92	255.88
FAR-Small <sup>†</sup>	20.3	3.90	11.59	83.19	244.49
DeiT-Base	86.5	17.56	55.49	283.77	928.02
FAR-Base	88.7	17.31	50.71	306.39	914.08
FAR-Base <sup>†</sup>	80.0	14.80	43.34	295.12	871.67

<sup>†</sup> Pruned model after structured compression.



Figure 4: Pruning ratios across heads and directions. FAR learns to prune differently across layers and directions, revealing internal heterogeneity in representational redundancy.

On  $224 \times 224$  inputs, the pruned FAR-Tiny achieves a 13.6% reduction in FLOPs (1.08G vs. 1.25G) and a 16.9% latency improvement on CPU (30.95ms vs. 26.51ms) compared to DeiT-Tiny. Similar trends hold for FAR-Small and FAR-Base, where the pruned models match or exceed the latency of their DeiT counterparts despite lacking highly parallelizable attention mechanisms. On higher-resolution inputs ( $384 \times 384$ ), the benefits become more pronounced: FAR-Tiny<sup>†</sup> is 13.4% faster on CPU and reduces compute by 32.6%. These results highlight the deployment potential of FAR under resource-constrained settings. Unlike attention, which suffers from quadratic complexity and memory bandwidth limitations on long sequences, FAR’s sequential architecture scales linearly and better utilizes compute on memory-bound platforms. The consistent gains after structured pruning further demonstrate that the LSTM substitutes remain efficient and compact when sparsified.

**Block-wise Adaptive Sparsity.** Our pruning method supports per-block, per-direction flexibility, enabling structured sparsity to emerge adaptively across the model. As shown in Figure 4, the pruning ratio varies substantially between forward and reverse LSTM modules, and across layers and heads. This aligns with the hypothesis that different blocks contribute unequally to representation quality and can be compressed to different extents. Previous work on ViT pruning [29] reports a high-low-high trend in pruning ratios across ViT blocks, which is also reflected in our results. This showcases the pruned architecture reflects the sensitivity of each block’s mapping function. Results for other model scales are available in Appendix B, showcasing similar behaviors.

**Effectiveness of Block-level Supervision.** We ablate different loss configurations to assess the importance of pretrained initialization and intermediate supervision. Table 3 reports the top-1 accuracy of FAR-Tiny under several training schedules. Training from scratch (TFS), without any distillation or teacher supervision, leads to suboptimal performance. For instance, relying solely on classification loss yields 70.4% accuracy, well below the 74.2% achieved with our proposed combined loss. Using similarity loss alone fails to converge, reaching only 64.3%, which highlights the difficulty of learning attention-equivalent behavior purely through representation matching.

In contrast, combining classification and similarity objectives consistently improves performance, indicating that block-level supervision provides essential guidance during training. Preliminary experiments on FAR-Small further support this trend: similarity-only variants underperform the combined objective, and classification-only training is hard to converge. These results align with our hypothesis that larger models benefit more from dense intermediate supervision, as replicating the inductive behavior of attention becomes harder to achieve with end-to-end signals alone.

Table 3: Top-1 accuracy under different loss configurations.

Schedule	TFS	Distill (cls)	Distill (sim)	Distill (combine)
FAR-Tiny	70.4	73.4	64.3	74.2
FAR-Small	63.6	77.3	72.8	77.9

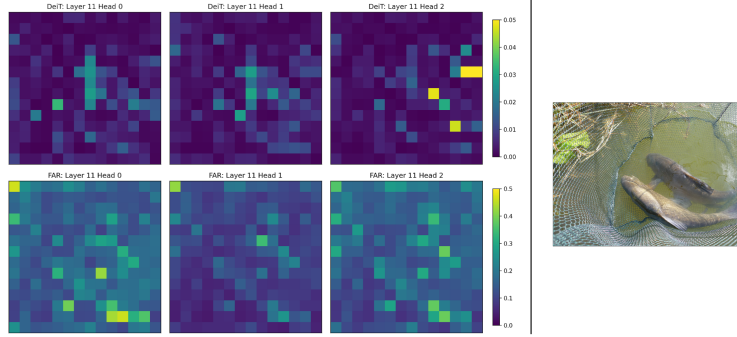


Figure 5: Token importance maps from DeiT (top) and FAR (bottom). Each head in FAR recovers distinct semantic regions without attention.

**Token-level Representation Consistency.** To examine whether the FAR modules preserve the structural behavior of attention, we visualize both CLS-token attention maps (Figure 5) and token-to-token dependencies (Figure 6). We use gradient saliency to compute the dependency for FAR.

Figure 5 shows that FAR learns to focus on semantically important regions, with each head capturing distinct spatial patterns similar to that of the attention model. Figure 6 compares token-to-token interaction heatmaps. Similar to attention, FAR identifies a sparse set of tokens that are mostly attended to by others. Meanwhile, FAR’s dependency map demonstrates a higher self-dependency and on neighboring tokens (illustrated by the bright near-diagonal region), which is as expected given the LSTM formulation. More results in Appendix C verify these observations.

## 5 Conclusion

We propose FAR, a function-preserving framework for attention replacement in pretrained transformers. By substituting attention blocks with learnable multi-head LSTM-based modules trained via block-wise distillation and global structural pruning, FAR maintains compatibility with pretrained transformer models. Extensive experiments on the DeiT family show that FAR preserves the classification accuracy of its attention-based counterparts across model scales and downstream tasks, while reducing FLOPs and latency. Notably, FAR retains the inductive structure and transferability of attention, as evidenced by token-to-token interaction visualizations and performance on domain transfer benchmarks. Our findings suggest that pretrained attention modules can be replaced with sequential architectures without retraining the full network, provided that proper structural

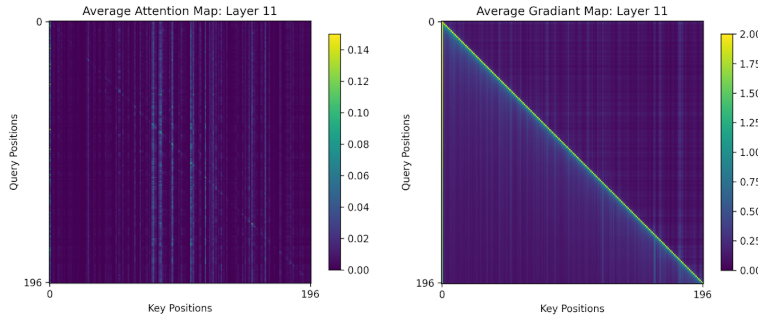


Figure 6: Token-to-token dependencies in DeiT (left) and FAR (right). Both models exhibit structured, sparse interactions with dominant positions.

supervision is applied. This opens new opportunities for deploying transformers in memory- and compute-constrained environments.

**Limitations.** Despite promising results, FAR exhibits several limitations. First, although we observe token sparsity in attention, we do not explicitly exploit this sparsity for further compression or routing. Second, our evaluation focuses on relatively short sequence lengths in vision classification tasks. Extending FAR to long-sequence applications such as vision-language models or autoregressive language modeling remains an open challenge, especially for LSTM-based models.

## Acknowledgments and Disclosure of Funding

The University of Arizona team thanks the supports of research collaboration grant and computation resources from TetraMem, Inc to this work. This work was based in part upon High Performance Computing (HPC) resources supported by the University of Arizona TRIF, UITS, and Research, Innovation, and Impact (RII) and maintained by the UArizona Research Technologies department.

## References

- [1] Ashish Vaswani, Noam Shazeer, Niki Parmar, Jakob Uszkoreit, Llion Jones, Aidan N. Gomez, Lukasz Kaiser, and Illia Polosukhin. Attention is all you need, 2023.
- [2] Jacob Devlin, Ming-Wei Chang, Kenton Lee, and Kristina Toutanova. Bert: Pre-training of deep bidirectional transformers for language understanding, 2019.
- [3] Alexey Dosovitskiy, Lucas Beyer, Alexander Kolesnikov, Dirk Weissenborn, Xiaohua Zhai, Thomas Unterthiner, Mostafa Dehghani, Matthias Minderer, Georg Heigold, Sylvain Gelly, Jakob Uszkoreit, and Neil Houlsby. An image is worth 16x16 words: Transformers for image recognition at scale, 2021.
- [4] Alec Radford, Jong Wook Kim, Chris Hallacy, Aditya Ramesh, Gabriel Goh, Sandhini Agarwal, Girish Sastry, Amanda Askell, Pamela Mishkin, Jack Clark, Gretchen Krueger, and Ilya Sutskever. Learning transferable visual models from natural language supervision, 2021.
- [5] Jean-Baptiste Cordonnier, Andreas Loukas, and Martin Jaggi. On the relationship between self-attention and convolutional layers, 2020.
- [6] Yi Tay, Mostafa Dehghani, Dara Bahri, and Donald Metzler. Efficient transformers: A survey, 2022.
- [7] Tri Dao, Daniel Y. Fu, Stefano Ermon, Atri Rudra, and Christopher Ré. Flashattention: Fast and memory-efficient exact attention with io-awareness, 2022.
- [8] Angelos Katharopoulos, Apoorv Vyas, Nikolaos Pappas, and François Fleuret. Transformers are rnns: Fast autoregressive transformers with linear attention. In *International conference on machine learning*, pages 5156–5165. PMLR, 2020.
- [9] Albert Gu and Tri Dao. Mamba: Linear-time sequence modeling with selective state spaces, 2024.
- [10] Christopher Wolters, Xiaoxuan Yang, Ulf Schlichtmann, and Toyotaro Suzumura. Memory is all you need: An overview of compute-in-memory architectures for accelerating large language model inference, 2024.
- [11] Xiaoxuan Yang, Bonan Yan, Hai Li, and Yiran Chen. Retransformer: Reram-based processing-in-memory architecture for transformer acceleration. In *2020 IEEE/ACM International Conference On Computer Aided Design (ICCAD)*, pages 1–9, 2020.
- [12] Shwai He, Guoheng Sun, Zheyu Shen, and Ang Li. What matters in transformers? not all attention is needed, 2024.

- [13] Srinadh Bhojanapalli, Ayan Chakrabarti, Andreas Veit, Michal Lukasik, Himanshu Jain, Frederick Liu, Yin-Wen Chang, and Sanjiv Kumar. Leveraging redundancy in attention with reuse transformers, 2021.
- [14] Sepp Hochreiter and Jürgen Schmidhuber. Long short-term memory. *Neural Computation*, 9(8):1735–1780, 1997.
- [15] Huanrui Yang, Wei Wen, and Hai Li. Deephoyer: Learning sparser neural network with differentiable scale-invariant sparsity measures, 2020.
- [16] Hugo Touvron, Matthieu Cord, Matthijs Douze, Francisco Massa, Alexandre Sablayrolles, and Hervé Jégou. Training data-efficient image transformers & distillation through attention, 2021.
- [17] Ilya Tolstikhin, Neil Houlsby, Alexander Kolesnikov, Lucas Beyer, Xiaohua Zhai, Thomas Unterthiner, Jessica Yung, Andreas Steiner, Daniel Keysers, Jakob Uszkoreit, Mario Lucic, and Alexey Dosovitskiy. Mlp-mixer: An all-mlp architecture for vision, 2021.
- [18] Yutao Sun, Li Dong, Shaohan Huang, Shuming Ma, Yuqing Xia, Jilong Xue, Jianyong Wang, and Furu Wei. Retentive network: A successor to transformer for large language models, 2023.
- [19] Albert Gu and Tri Dao. Mamba: Linear-time sequence modeling with selective state spaces. *arXiv preprint arXiv:2312.00752*, 2023.
- [20] Sinong Wang, Belinda Z. Li, Madian Khabsa, Han Fang, and Hao Ma. Linformer: Self-attention with linear complexity, 2020.
- [21] Krzysztof Choromanski, Valerii Likhoshesterov, David Dohan, Xingyou Song, Andreea Gane, Tamas Sarlos, Peter Hawkins, Jared Davis, Afroz Mohiuddin, Lukasz Kaiser, David Belanger, Lucy Colwell, and Adrian Weller. Rethinking attention with performers, 2022.
- [22] Tri Dao, Daniel Y. Fu, Stefano Ermon, Atri Rudra, and Christopher Ré. Flashattention: Fast and memory-efficient exact attention with io-awareness, 2022.
- [23] Nikita Kitaev, Łukasz Kaiser, and Anselm Levskaya. Reformer: The efficient transformer, 2020.
- [24] Geoffrey Hinton, Oriol Vinyals, and Jeff Dean. Distilling the knowledge in a neural network, 2015.
- [25] Xiaoqi Jiao, Yichun Yin, Lifeng Shang, Xin Jiang, Xiao Chen, Linlin Li, Fang Wang, and Qun Liu. Tinybert: Distilling bert for natural language understanding, 2020.
- [26] Zhiqing Sun, Hongkun Yu, Xiaodan Song, Renjie Liu, Yiming Yang, and Denny Zhou. Mobilebert: a compact task-agnostic bert for resource-limited devices, 2020.
- [27] Wenhui Wang, Furu Wei, Li Dong, Hangbo Bao, Nan Yang, and Ming Zhou. Minilm: Deep self-attention distillation for task-agnostic compression of pre-trained transformers, 2020.
- [28] Angela Fan, Edouard Grave, and Armand Joulin. Reducing transformer depth on demand with structured dropout, 2019.
- [29] Huanrui Yang, Hongxu Yin, Maying Shen, Pavlo Molchanov, Hai Li, and Jan Kautz. Global vision transformer pruning with hessian-aware saliency. In *Proceedings of the IEEE/CVF conference on computer vision and pattern recognition*, pages 18547–18557, 2023.
- [30] Hongxu Yin, Arash Vahdat, Jose M Alvarez, Arun Mallya, Jan Kautz, and Pavlo Molchanov. A-vit: Adaptive tokens for efficient vision transformer. In *Proceedings of the IEEE/CVF conference on computer vision and pattern recognition*, pages 10809–10818, 2022.
- [31] Jia Deng, Wei Dong, Richard Socher, Li-Jia Li, Kai Li, and Li Fei-Fei. Imagenet: A large-scale hierarchical image database. In *2009 IEEE Conference on Computer Vision and Pattern Recognition*, pages 248–255, 2009.
- [32] Alex Krizhevsky. Learning multiple layers of features from tiny images. Technical report, University of Toronto, 2009.

- [33] Jonathan Krause, Michael Stark, Jia Deng, and Li Fei-Fei. 3d object representations for fine-grained categorization. In *Proceedings of the IEEE Conference on Computer Vision and Pattern Recognition (CVPR)*, pages 554–561, 2013.
- [34] M-E Nilsback and A Zisserman. Automated flower classification over a large number of classes. In *Proceedings of the Indian Conference on Computer Vision, Graphics and Image Processing*, pages 722–729, 2008.

## A Training Schedules and Hyperparameters

This appendix provides detailed training settings and learning rate schedules used in all experiments, including baseline and pruned models.

### A.1 Setups in Distillation

This section details the hyperparameter configurations used in the distillation and finetuning stages of FAR training. All experiments use the AdamW optimizer with a weight decay of 0.05 and  $\beta$  values set to their PyTorch default if unspecified. Unless otherwise noted, dropout is disabled ( $p = 0$ ), and the drop path rate is set to 0.1. No gradient clipping is applied during training.

In the distillation phase, only the LSTM-based attention substitutes are trainable, while all other components are frozen. Models are trained for 200 epochs using a cosine learning rate scheduler with 5 warmup epochs. The base learning rate is  $5 \times 10^{-4}$ , and the warmup starting learning rate is  $1 \times 10^{-5}$ . All models use a global batch size of 256.

In the subsequent finetuning phase, all parameters are unfrozen and jointly optimized using only classification loss. Finetuning lasts 100 epochs. The learning rate is set to  $5 \times 10^{-5}$  for DeiT-Tiny, and  $2 \times 10^{-5}$  for DeiT-Small and DeiT-Base.

To ensure training consistency across scales, we use 1, 2, and 4 GPUs respectively for DeiT-Tiny, DeiT-Small, and DeiT-Base, and apply linear scaling to batch size and learning rate accordingly. All experiments are trained with DistributedDataParallel (DDP) and use automatic mixed precision (AMP).

### A.2 Setups in Pruning

This section describes the training settings used during the structured pruning stage of FAR. The pruning process is applied to all layers of the LSTM substitute modules using DeepHoyer regularization, targeting the hidden dimension of each head in both the forward and backward directions. The regularization loss is added to the classification objective, weighted by a coefficient of  $10^{-4}$ . The pruning threshold is set to  $10^{-4}$  and used for magnitude-based channel selection.

Pruning is performed for 100 epochs using the AdamW optimizer, with a cosine learning rate schedule and 5 warmup epochs. The learning rate is set to  $5 \times 10^{-5}$  for DeiT-Tiny, and  $5 \times 10^{-6}$  for DeiT-Small and DeiT-Base. A fixed batch size of 256 is used for all models. No gradient clipping is applied. Unless otherwise specified, other hyperparameters follow the same configuration as in the distillation stage.

After pruning, we optionally perform a 100-epoch finetuning stage using the same optimizer and batch size. The learning rate during finetuning matches that used in the pruning stage for each model scale. All parameters—including the LSTM blocks and surrounding layers—are unfrozen and jointly optimized during pruning and finetuning. Random seed is fixed for all runs to ensure reproducibility.

### A.3 Setups in Downstream

This section outlines the training configurations used for downstream finetuning. Unlike the distillation stage, we do not retrain the attention substitutes using block-wise supervision. Instead, we directly finetune the FAR models—pretrained on ImageNet—on each downstream dataset using standard task supervision.

All downstream experiments use the AdamW optimizer with a fixed learning rate of  $5 \times 10^{-5}$  and a cosine learning rate schedule with 5 warmup epochs. Unless otherwise noted, the remaining training settings are consistent with those used in the distillation phase.

For CIFAR-10, CIFAR-100, Stanford Cars, and Flowers-102, we train for 1000 epochs. During these runs, we disable stochastic depth ('drop-path') and token-level reprob augmentation for stability, following the downstream protocol in DeiT [16]. For iNaturalist datasets (iNat18 and iNat19), we train for 360 epochs using the same augmentation pipeline as used in ImageNet pretraining and distillation. All downstream experiments use full-model finetuning with all parameters unfrozen.

#### A.4 Other Setups

All latency measurements are conducted on an AMD EPYC 9254 24-Core CPU using ONNX Runtime (ORT). Since most inference optimization libraries are better optimized for attention-based architectures than for sequential models such as LSTMs, we apply explicit system-level constraints to ensure fair and deterministic comparisons. Specifically, we disable CPU memory arena management via `ORT_ENABLE_CPU_MEM_ARENA=0`, restrict execution to a single thread using `OMP_NUM_THREADS=1`, and limit CPU instruction set to AVX2 by setting `DNNL_MAX_CPU_ISA=AVX2`. Thread affinity and memory locality are controlled via `OMP_PROC_BIND=TRUE`, `OMP_PLACES=cores`, and `numactl -physcpubind=0 -membind=0`.

We report latency as the median wall-clock time of 100 inference runs on a single image and a single head. Before each measurement, we perform 30 warmup runs to account for cache effects and dynamic initialization. The entire measurement process is repeated multiple times, and the final latency is averaged across runs.

#### B Pruned Model Structures Across Scales

To complement the visualization in the main paper, we present the head-wise pruning ratios for DeiT-Small and DeiT-Base in Figure 7 and Figure 8, extending the structural analysis beyond DeiT-Tiny. Each heatmap shows the percentage of retained hidden units in the LSTM block after structured pruning, for both the forward and reverse directions.

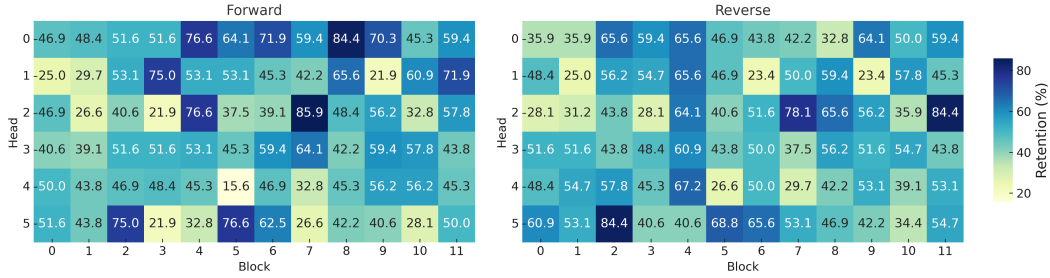


Figure 7: Retention ratios of each LSTM head after pruning on FAR-Small. Values denote the percentage of non-zero hidden units retained after DeepHoyer pruning.

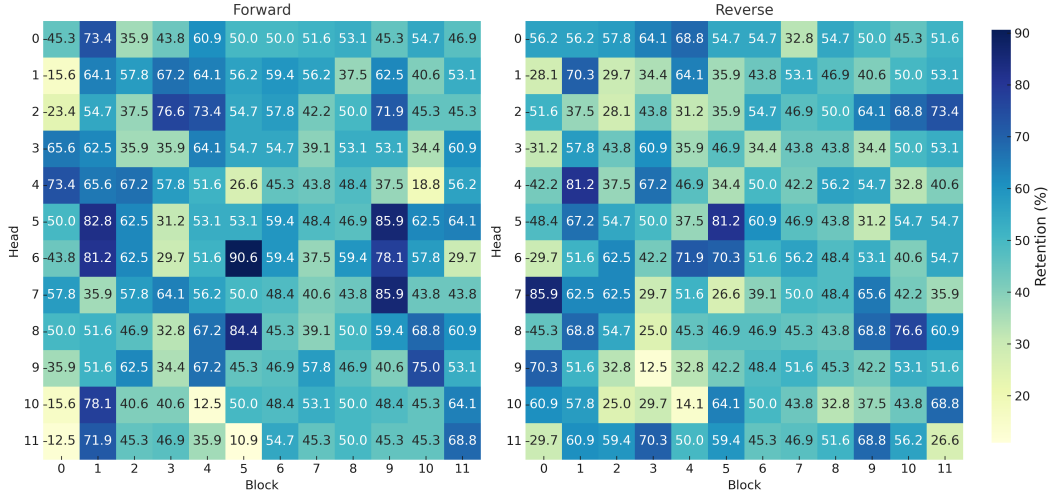


Figure 8: Retention ratios of each LSTM head after pruning on FAR-Base. Values denote the percentage of non-zero hidden units retained after DeepHoyer pruning.

As shown, the pruning patterns exhibit significant variation across both blocks and heads. Across both scales, we observe consistent heterogeneity in sparsity across heads, layers, and directions. Deeper layers tend to retain more units, particularly in the reverse direction, suggesting higher representational

demand. This observation is consistent with the trend seen in DeiT-Tiny and confirms the necessity of adaptive pruning per block and direction. Uniform sparsity or fixed global thresholds would likely over-prune key heads or under-utilize redundancy in shallower layers. We also observe that the forward and reverse directions exhibit different sparsity patterns in most layers, often retaining complementary sets of heads. This structural asymmetry reinforces the need for direction-specific pruning rather than symmetric treatment of bidirectional units. This anisotropy becomes more prominent as model scale increases, suggesting that larger architectures benefit from more flexible channel allocation.

These results confirm the necessity of block-wise and direction-wise adaptive pruning. Uniform sparsity levels would ignore head-level importance and may lead to suboptimal retention in capacity-critical layers. Our use of DeepHoyer regularization with local thresholding enables the model to retain important substructures while reducing redundancy, contributing to the overall efficiency of FAR without sacrificing alignment with the pre-trained attention structure.

## C Token-to-token Importance Visualization Analysis

This appendix provides a layer-wise qualitative analysis comparing the internal token interaction patterns learned by our attention-free replacement (FAR) modules and the original attention heads in DeiT. Specifically, we visualize head-wise attribution maps from the CLS token to patch tokens across multiple layers, aiming to assess whether FAR can recover structured attention behavior through block-level distillation.

We visualize the interaction patterns between the CLS token and the input patch tokens by aggregating either:

- the softmax-normalized attention weights in DeiT, or
- the gradient-based input-output attribution scores in FAR, computed via cumulative back-propagation from the CLS token.

Since attention explicitly computes pairwise similarity while FAR uses a recurrent LSTM structure, direct comparability is imperfect. However, visual similarity in structural focus and sparsity can serve as an indicator of alignment.

### C.1 CLS-to-patch Analysis

We select three representative layers from DeiT-Tiny: Layer 0 (shallow), Layer 5 (intermediate), and Layer 7 (deep). These layers reflect different stages of representation formation. We visualize the three heads per layer (Figure 9, Figure 10 and Figure 11), for both DeiT and FAR models trained with global attention replacement and block-wise supervision.

**Layer 0: Localized focus in FAR.** As shown in Figure 9, while DeiT attention exhibits relatively uniform soft focus across all patches, FAR’s attributions are highly concentrated in the top-left region (neighboring tokens). This reflects the sequential and autoregressive nature of LSTM: since the CLS token appears at the beginning of the token sequence, it can only incorporate information from future tokens in the forward pass, leading to initial local activation.

**Layer 5: Emerging structural alignment.** Figure 10 illustrates attribution in the intermediate layer. At this stage, while DeiT exhibits localized attention with spatially distinct peaks, FAR gradually begins to form similar token interaction patterns, especially in Head 0. Compared to its behavior in shallow layers, FAR shows more structured and spread-out attribution in mid layers. The FAR module begins to exhibit more balanced and structured patterns, with multiple heads showing diagonally symmetric or regionally aggregated activations. While minor intensity scaling differences remain (due to attribution vs. normalized attention), the spatial layout of activations shows clear resemblance.

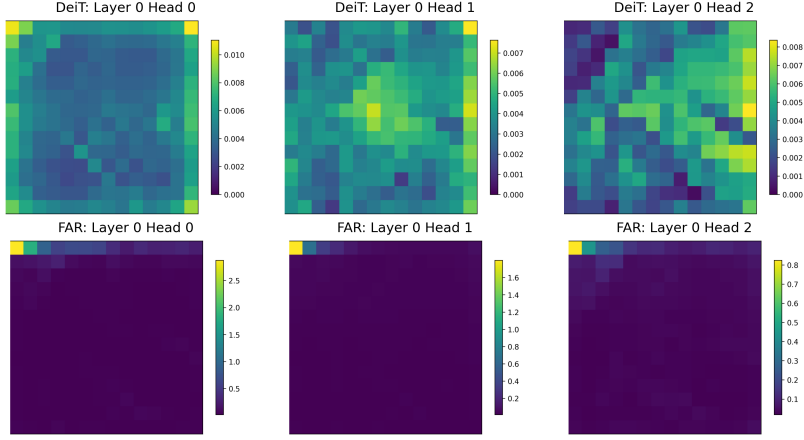


Figure 9: CLS-to-patch attribution maps in Layer 0 for three heads. FAR (bottom) displays strong left-biased sparsity due to sequential computation, while DeiT (top) exhibits uniform spatial spread.

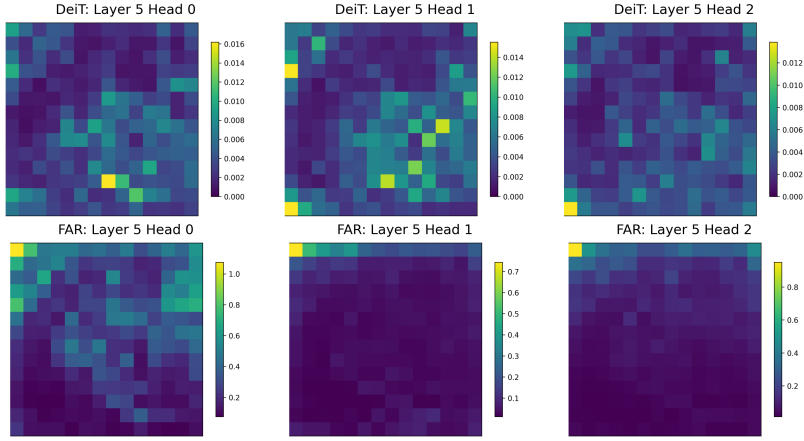


Figure 10: CLS attribution in Layer 5. FAR heads display early signs of global context encoding, resembling the spatial layout of attention heads in DeiT.

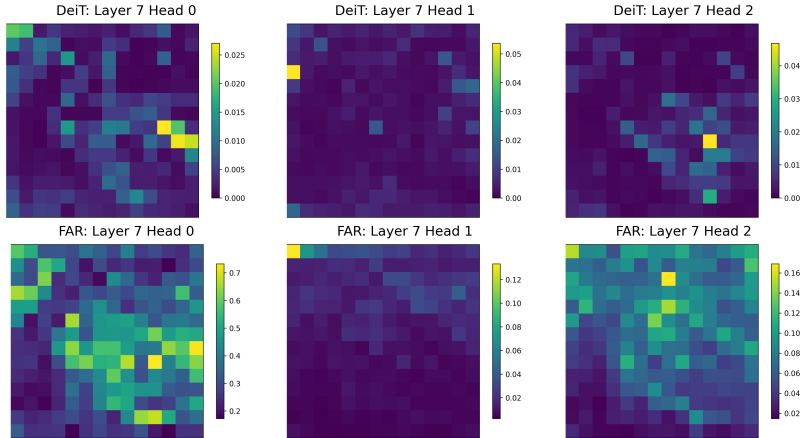


Figure 11: Layer 7 attribution maps show high structural agreement between DeiT and FAR, confirming the convergence of interaction modeling in deeper layers.

**Layer 7: Strong convergence in deep layers.** By Layer 7, the attribution maps in Figure 11 in FAR and DeiT become highly similar in structural distribution, even though FAR lacks attention. Heads in both models capture semantically salient regions and sparse dominant patch tokens, confirming that block-level supervision suffices to drive global structure learning in FAR.

**Interpretation and Insights** We observe that the left-localized bias in FAR’s shallow layers is not a flaw, but a direct consequence of sequential computation and the positional arrangement of the CLS token. As depth increases, stacked LSTM modules gain access to broader context and learn to redistribute attention via implicit gradients. The progressive emergence of alignment validates the effectiveness of block-level distillation, even without explicit token-level supervision. The remaining gap in early layers suggests that incorporating layer-wise or head-wise alignment losses may further improve fine-grained behavior matching.

## C.2 Token-wise Dependency Analysis

Besides CLS token visualization, we also visualized token-level interactions by examining full token-to-token dependency matrices in DeiT and FAR across three representative layers: Layer 0 (shallow), Layer 5 (intermediate), and Layer 7 (deep). These heatmaps (Figure 12, Figure 13 and Figure 14) provide a global view of the spatial sparsity and dependency patterns beyond CLS-centric attention.

Similar to Section C.1, for DeiT, we compute the average attention matrix across all heads and samples in a given layer. For FAR, which lacks explicit attention scores, we approximate token-level dependencies by computing cumulative input-output gradient attribution for each token position.

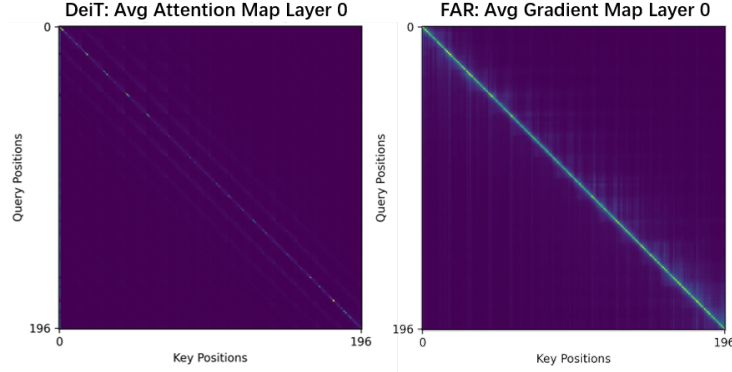


Figure 12: Token-to-token dependency heatmaps in Layer 0. DeiT (left) shows moderate locality; FAR (right) is strongly diagonal due to sequential access.

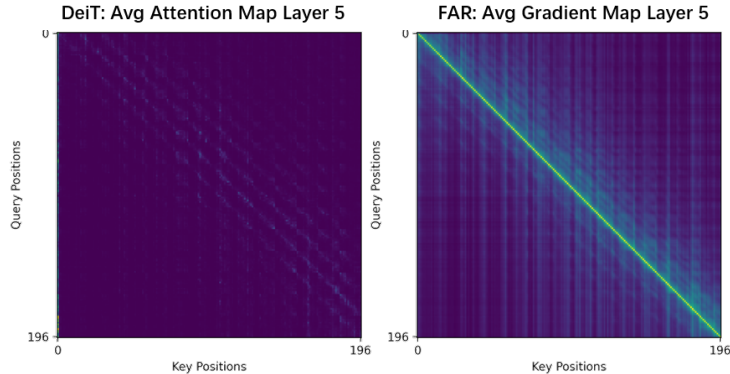


Figure 13: Token-to-token interaction in Layer 5. DeiT attention is broader and distributed; FAR shows sparse diagonals capturing long-range dependencies.

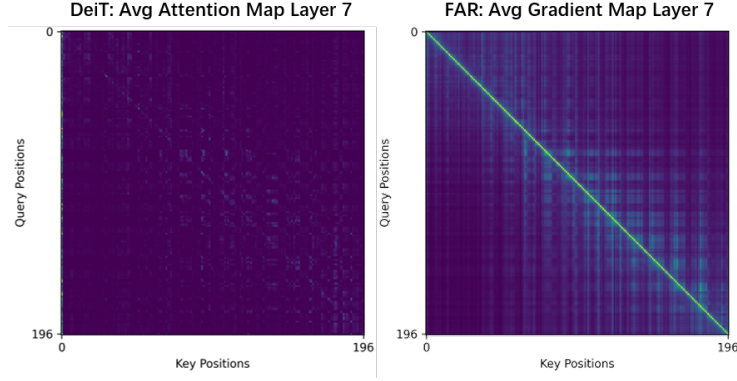


Figure 14: Layer 7 token dependencies. FAR develops sparse but structured attention-like focus, while DeiT remains dense.

**Layer 0: Localized Dependencies.** As shown in Figure 12, both DeiT and FAR exhibit strong locality bias in shallow layers. Tokens tend to focus on their immediate neighbors, forming diagonal patterns. This reflects inductive locality in attention and the causal left-to-right accumulation in FAR’s recurrent dynamics. DeiT displays more horizontally diffused attention, while FAR remains concentrated due to limited receptive field in early LSTM layers.

**Layer 5: Emergence of Structured Diagonals and Cross-axis Patterns.** In the intermediate stage (Figure 13), both DeiT and FAR begin to exhibit more structured token interactions. Multiple soft diagonals appear in both models, indicating increasing capacity to capture relative positional patterns beyond immediate neighbors. In addition, early signs of horizontal and vertical activations emerge, particularly in FAR, suggesting the model begins to identify key tokens with global influence. Compared to DeiT, FAR displays sparser but sharper activations along both diagonals and axes, reflecting its memory-based sequential processing and tendency toward sparse long-range dependency.

**Layer 7: Dominance of Axis-wise Interactions with Residual Diagonal Focus.** By the final block (Figure 14), both models demonstrate global token integration with clear vertical and horizontal activation bands. This reflects the identification of dominant query and key positions, possibly corresponding to semantically important regions. While DeiT’s diagonals weaken and the map becomes more diffuse, FAR retains a consistent diagonal structure due to its inherently sequential nature. The combination of axis-wise sparsity and preserved diagonality suggests that FAR captures a distinct hybrid pattern of both content-based salience and relative positional bias.

These findings support our hypothesis that block-wise distillation enables FAR to gradually approximate the global mapping behavior of attention layers. While early FAR layers reflect sequential bias, deeper layers exhibit meaningful token-to-token alignment and structured sparsity. This also opens future avenues for leveraging such sparsity for further acceleration or compression.